Multidisciplinary Research Journal
ISSN (online): 3108 – 1533

Volume 2, Issue 1, 2026
January – March 2026

Research Article

DFT Study of Pressure-Dependent Elastic Properties of α-ZnP_2

Sushil Rajpurohit [1,*], **Ghanshyam Sharma** [2]

[1] Vardhman Mahaveer Open University, Kota, Rajasthan, INDIA-324010
[2] University of Kota, Kota, Rajasthan, INDIA- 324005
* Correspondence: sushilrajpurohit21@gmail.com

Scopus Author ID 57219344213

Received: 5 September 2025; Accepted: 30 March 2026; Published: 29 April 2026

Abstract: The article explores pressure-dependent elastic properties of α-ZnP_2 for the pressure range of 0-10 GPa. The investigation is carried out with the CRYSTAL Code and the ELATE software. The present study reveals that bulk modulus has a higher sensitivity to pressure than Young's modulus and shear modulus. The difference between G_{max} and G_{min} for the values of shear modulus G increases with an increase in pressure. Poisson's ratio (ν_H) experiences change about 39% as pressure changes from zero to 10 GPa. As pressure increases, the universal elastic anisotropy index (A^U) and log-Euclidean anisotropy index (A^L) increase. Directional-dependent characteristics of Young's modulus and linear compressibility have been examined with polar plots in different crystallographic planes. This study shows that elastic anisotropy of α-ZnP_2 increases with pressure.

Keywords: Anisotropy; Elastic; Linear compressibility; Young's modulus

1. Introduction

The Zn-P system has a few binary phases, such as ZnP_2, ZnP_4 and Zn_3P_2 [1]. The formation of binary phases is largely dependent on the Zn/P composition, pressure and temperature of the system [2–3]. II-V_2 semiconductor materials have been immensely investigated because of their technological applications. Two distinct crystalline phases of ZnP_2 are α-ZnP_2 (tetragonal) and β-ZnP_2 (monoclinic) [4–5]. A tetragonal crystal structure of α-ZnP_2 was reported by White [6] and Stackelberg *et al.* [7]. The crystal structure of α-ZnP_2 was also confirmed through experiments by Zanin *et al.* in 2003 [8]. The melting point of the α-ZnP_2 is 985±1°C [9].

The studies of various properties of binary zinc phosphides have thrived through density functional theory-based research [10–15]. Binary zinc phosphides are useful in the fabrication of sodium-ion battery anodes having high performance [16]. As stated by Nam *et al*., carbon-modified composite (ZnP_2-C) may be a probable promising alternative as a high-performance SIB (sodium ion battery) anode substance in view of its notable electrochemical sodium-storage characteristics [16]. Ji *et al.* selected zinc phosphide composite to serve as a PIB (Potassium–Ion Batteries) anode [17]. In view of specific intrinsic characteristics, it serves as a dielectric in metal-insulator-semiconductor (MIS) devices [8]. ZnP_2 is a propitious substance for applications in semiconductor optoelectronics and nonlinear optics [18]. The potencies of controlling the particularities of photodiodes through gyration properties in ZnP_2-D_4^8 crystals were attained [19]. The layer of ZnP_2-D_4^8 in photodetectors may be utilised for rotation of the polarisation plane of incoming light [20]. It has favorable inherent characteristics, including relatively large band gaps and anisotropic optical properties with

significant birefringence [18]. These characteristics enable the use of ZnP_2 for fabricating microelectronic elements, photodetectors for laser radiation, photoresistors, etc. [18].

In this present investigation, a comprehensive examination of elastic properties has been undertaken. To the best of our knowledge, the elastic anisotropy and elastic properties of α-ZnP_2 under pressure have not been reported. The present research work will enrich the understanding of macroscopic details about direction-dependent elastic properties of α-ZnP_2 under pressure. An exhaustive knowledge of elastic anisotropy has notable importance for deciding the preferred crystallographic orientation of the crystals in device design to achieve optimum performance.

2. Computational Details

Elastic properties of the α-ZnP_2 are investigated with the CRYSTAL package (periodic *ab initio* HF and DFT code) [21–22]. The α-ZnP_2 has 08 formula units in the unit cell [4, 6]. Thus, α-ZnP_2 has 24 atoms in the unit cell [4]. The properties of the alpha phase of ZnP_2 with space group $P4_32_12$ [4, 6] are investigated through DFT. A restricted closed-shell KS (Kohn-Sham) Hamiltonian-type calculation is used [22]. In the present study, calculations are performed with the DFT exchange-correlation functional GGA (Generalised Gradient Approximation). The computations of geometry optimisation using initial geometry [6] and elastic properties [23–25] are performed with the PBE scheme [26–27]. In this present computational research, we utilise the basis sets for zinc and phosphorus atoms from the CRYSTAL-Basis Set Library of the Torino group [21–22, 28–29]. The convergence threshold TOLDEE on energy is adopted at 10^{-8} Hartree. For carrying out prompt convergence, the BROYDEN accelerator scheme [21–22, 30–31] is utilised. The Fock/KS matrix mixing factor (namely, FMIXING keyword) has been employed as a convergence tool for the computations. An 8×8×8 k-points (Monkhorst-Pack) mesh [32] is implemented for computations. The size of the strain step for the investigation of elastic computations is 0.01. RMS of the gradient parameter TOLDEG has a default value of 0.0003 a.u. [22]. RMS of the displacement parameter TOLDEX has a default value of 0.0012 a.u. [22]. A constant pressure preoptimisation parameter (namely, PREOPTGEOM keyword) is employed in accomplishing the computational investigation of the elastic stiffness coefficients for various pressures.

Elastic tensor $C_{\alpha\beta}$ may be expressed in terms of strain second derivatives of total energy E as [22, 25, 33] shown in Eq. (1)

$$C_{\alpha\beta} = \frac{1}{V}\frac{\partial^2 E}{\partial\varepsilon_\alpha \partial\varepsilon_\beta}\bigg|_0 \tag{1}$$

where, ε is the second-rank symmetric tensor of pure strain, $\alpha, \beta = 1, 2, ..., 6$ as per Voigt's notation.

In the lack of any finite pre-stress, the above expression as provided in Eq. (1) is used for 3D crystal system in the CRYSTAL code.

The ELATE software [34–35] is also utilised for the computations of maximum and minimum values of different elastic quantities. ELATE is open source software.

3. Results and Discussion

At zero pressure, equilibrium lattice parameters of α-ZnP_2 are a_0=5.108 Å and c_0=18.620 Å [36]. Obtained optimised lattice parameters are a=4.897 Å and c=17.960 Å at a pressure of 10 GPa. Equilibrium ratios are (a/a_0)=0.959 and (c/c_0)=0.965. It shows that decrement in the (a/a_0) is slightly greater than that of (c/c_0), as pressure increases. Crystal planes (001), (010) and (100) are important as they are symmetry planes. Crystal planes (001) and (010) of α-ZnP_2 are shown in Figure 1. CRYSPLOT [37–38] is used for plotting the Figure 1 which is based on computations from CRYSTAL Code [21–22]. CRYSPLOT is an online free tool [37–38].

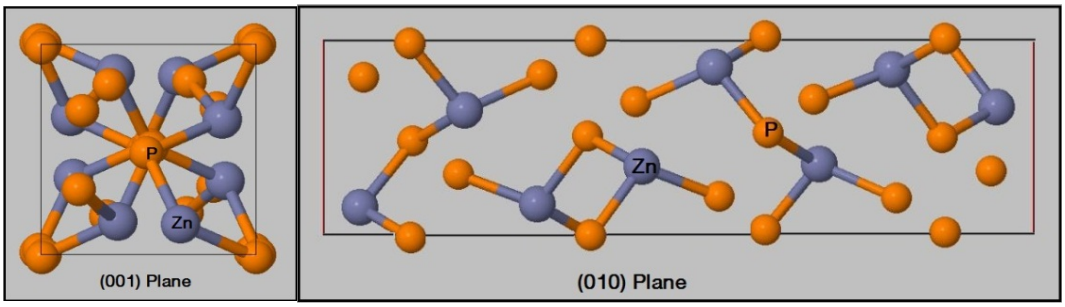

Figure 1. (001) and (010) planes of α-ZnP_2 at zero pressure

3.1. Elastic stiffness constants and elastic quantities

Elastic stiffness constants have significant importance in dealing with principles of mathematical stress analysis and design. The elastic stiffness coefficients can predict the elastic behavioral response of materials to exerting stress. The alpha phase of ZnP_2 crystal has 06 independent elastic stiffness constants, namely C_{11}, C_{33}, C_{44}, C_{66}, C_{12} and C_{13} as it belongs to tetragonal (I) class (4/mmm) [33]. Computational materials science has vital importance in exploring elastic properties of materials. Table 1 displays the elastic stiffness constants of α-ZnP_2 crystal. Data of Table 1 are utilised in subsequent sections of the present article for computations/plots, such as elastic anisotropy parameters, various elastic moduli, polar graphs, etc.

Table 1. Computed C_{ij} elastic stiffness constants (in GPa) of α-ZnP_2 at pressure P (in GPa) together with other researchers' work

	P	C_{11}	C_{12}	C_{13}	C_{33}	C_{44}	C_{66}
Previous work[a]	0	108.21	46.66	42.39	118.78	44.92	62.04
Other theo. work[b]		116.48	54.18	48.12	126.37	44.34	59.42
Other theo. work[c]		118.00	53.00	45.00	123.00	45.00	60.00
Other exp. work[d]		102.10	30.76		115.70	42.85	52.08
Present work	2	116.45	55.09	51.11	130.57	46.34	63.66
Present work	4	124.35	63.89	59.97	139.62	46.71	64.82
Present work	6	131.95	72.71	68.77	147.36	46.92	65.71
Present work	8	139.64	81.52	77.68	154.74	46.74	66.24
Present work	10	146.67	89.96	85.99	161.73	46.20	66.48

[a]Ref. [36], [b]Ref. [12], [c]Ref. [13], [d]Ref. [39]

According to Mouhat and Coudert [40], for the crystal of the tetragonal (I) class (4/mmm), the four necessary as well as sufficient elastic stability criteria may be shown as Eqs. (2-5)

$$\left|C_{12}\right| < C_{11} \tag{2}$$

$$C_{13}^2 < \frac{1}{2} C_{33}\left(C_{11} + C_{12}\right) \tag{3}$$

$$C_{44} > 0 \tag{4}$$

$$C_{66} > 0 \tag{5}$$

According to our information, neither theoretical nor experimental studies on elastic stiffness constants of α-ZnP_2 for higher pressures (range up to 10 GPa) have been made. The computed C_{ij} (elastic stiffness constants) of the α-ZnP_2 crystal fulfil these necessary as well as sufficient elastic stability criteria. Hence, our result states the mechanical stability of α-ZnP_2 crystal in the pressure range from zero to 10 GPa.

Table 1 illustrates that coefficients C_{33} and C_{11} are significantly greater than the other coefficients, such as C_{12}, C_{13}, C_{44} and C_{66}. Table 1 also describes that variations in values of C_{11}, C_{12}, C_{13} and C_{33} are intensely dependent on pressure, whereas C_{44} and C_{66} do not show substantial variation in their values with applied pressure. Figure 2(a) describes that both values of C_{12} and C_{13} are less than C_{66} at zero pressure. However, both the values of C_{12} and C_{13} are greater than C_{66} at higher pressures (as per Table 1), as the effects of increasing pressure result in raising the values of C_{12} and C_{13}. The values of C_{12} and C_{13} rise almost linearly with hydrostatic pressure.

For the tetragonal (I) class (4/mmm) crystal, Reuss bulk modulus B_R, Reuss shear modulus G_R, Voigt bulk modulus B_V and Voigt shear modulus G_V may be expressed as [41–43] Eqs (6-9)

$$B_R = \left[S_{33} + 2S_{11} + 2S_{12} + 4S_{13}\right]^{-1} \tag{6}$$

$$G_R = 15\left[3\left(S_{66} + 2S_{44}\right) + 4\left(S_{33} + 2S_{11}\right) - 4\left(S_{12} + 2S_{13}\right)\right]^{-1} \tag{7}$$

$$B_V = \frac{C_{33} + 2C_{11} + 2C_{12} + 4C_{13}}{9} \tag{8}$$

$$G_V = \frac{1}{5}\left[C_{66} + 2C_{44}\right] + \frac{1}{15}\left[C_{33} - C_{12} + 2C_{11} - 2C_{13}\right] \tag{9}$$

where S_{ij} denotes elastic compliance coefficients.

Elastic tensor $\boldsymbol{C}$ and compliance tensor $\boldsymbol{S}$ are related as $\boldsymbol{C} = \boldsymbol{S}^{-1}$
For tetragonal crystal system [33], the expressions are provided by Eqs. (10-16) as below.

$$C_{11} + C_{12} = S_{33} / S \tag{10}$$

$$C_{11} - C_{12} = 1/\left(S_{11} - S_{12}\right) \tag{11}$$

$$C_{13} = -S_{13}/S \tag{12}$$

$$C_{33} = \left(S_{11} + S_{12}\right)/S \tag{13}$$

$$C_{44} = 1/S_{44} \tag{14}$$

$$C_{66} = 1/S_{66} \tag{15}$$

$$S = S_{33}(S_{11} + S_{12}) - 2S_{13}^2 \tag{16}$$

As per the Voigt-Reuss-Hill method, macroscopic polycrystalline Young's modulus E_H, Poisson's ratio ν_H, bulk modulus B_H and shear modulus G_H may be expressed as (Eqs. 17-20) [41–43].

$$G_H = \frac{1}{2}\left[G_R + G_V\right] \tag{17}$$

$$B_H = \frac{1}{2}\left[B_R + B_V\right] \tag{18}$$

$$\nu_H = \frac{1.5B_H - G_H}{G_H + 3B_H} \tag{19}$$

$$E_H = \frac{9G_H B_H}{G_H + 3B_H} \tag{20}$$

Using data of Table 1 in the present work, the density ρ and different elastic quantities (B, G, E and ν) at various pressure values are estimated as depicted in Table 2. Elastic stiffness constants contribute to the analysis of the strength of crystals. The values of Young's modulus predict the sufficient mechanical strength of α-ZnP_2. The characteristics of these key physical properties are useful in specific industrial applications. The orthorhombic crystal of phosphorus has bulk modulus of ≅36 GPa [44] and Young's modulus of 30.4 GPa [45]. The bulk modulus and Young's modulus for Zn crystal are 60.6 GPa and 92.7 GPa, respectively [45]. In the pressure range 0-10 GPa, the calculated values of bulk modulus and Young's modulus of the alpha phase of ZnP_2 exceed those of the respective mentioned values of its constituent elements.

The bulk modulus is related to resistance to volume change and shear modulus is related to resistance to shear stress. For α-ZnP_2, bulk modulus is substantially greater than shear modulus. Therefore, α-ZnP_2 serves higher resistance to volume change than shape change. Bulk modulus B_0 at temperature 295 K is about 444 GPa for diamond and about 98 GPa for silicon [45]. Therefore, bulk modulus (~ 66.4 GPa) of α-ZnP_2 is also less than that of silicon.

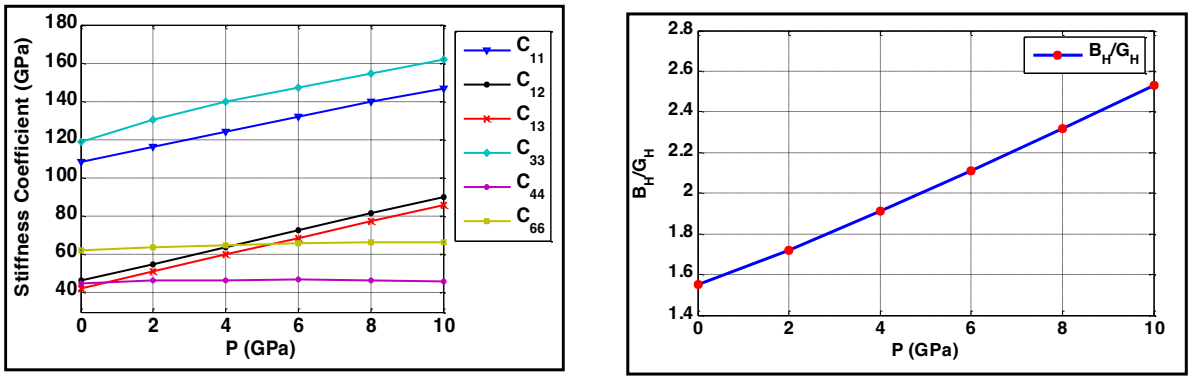

(a) **(b)**

Figure 2. (a) Variation of elastic stiffness constants (C_{ij}) with pressure P; **(b)** ratio of bulk modulus to shear modulus (B_H/G_H) at various pressure

Soshnikov *et al.* [39] measured B and G of α-ZnP_2 as 63.6 GPa and 39.3 GPa, respectively, which are based on the ultrasonic experimentations. Table 2 shows that B_H follows a substantial variation with pressure. In the case of ratio B/G greater than a value of approximately 1.75 [46], the malleable sort of nature of polycrystalline material is expected. It is therefore important to examine the ratio B/G for α-ZnP_2. The value of B/G is nearly 1.55 at zero pressure; hence, it indicates the brittle type of nature of α-ZnP_2 [36]. Brittle materials are prone to abrupt cracking once a certain directional stress limit is exceeded. The ratio B/G varies almost in a linear manner with pressure in the pressure range 0 to 10 GPa. Figure 2(b**)** depicts that values of B/G greater than a value of 1.75 take place for pressure greater than around 2.3 GPa; therefore, the malleability of α-ZnP_2 increases with increasing pressure. The increasing values of B/G with hydrostatic pressure illustrate the improvement in malleability with increasing pressure. Table 2 reveals that values of Poisson's ratio change from 0.235 to 0.326 as pressure varies from zero to 10 GPa. Thus, it is apparent that calculated values of v exist in the theoretically expected range values [47] for materials.

Table 2. Values of bulk modulus B (in GPa units), shear modulus G (in GPa units), density ρ (in g/cm^3 units), Young's modulus E (in GPa units) and Poisson's ratio v (unitless) of α-ZnP_2. Present work under PBE scheme according to Voigt-Reuss-Hill notations

	P	B_H	G_H	E_H	v_H	ρ
Previous work[e]	0	66.43	42.80	105.70	0.235	3.442
Other theo. work[f]		73.34	42.61	107.07		3.496
Present work	2	75.29	43.73	109.91	0.257	3.556
Present work	4	83.94	43.87	112.09	0.277	3.647
Present work	6	92.35	43.77	113.40	0.295	3.730
Present work	8	100.80	43.44	113.96	0.312	3.808
Present work	10	108.71	42.92	113.78	0.326	3.883

[e]Ref. [36], [f]Ref. [12]

3.2. Elastic anisotropy

Elastic anisotropy plays a pivotal role in technological implementations. Elastic anisotropy guides in ascertaining the appropriate crystal orientation to achieve improved performance with greater mechanical durability. The anisotropic elasticity of crystal affects their mechanical behavior. Using a DFT study, elastic anisotropy of materials may be revealed.

In this investigation, directional-dependent variations in Young's modulus E and linear compressibility β for α-ZnP_2 crystal have been studied. In the case of a crystal of the tetragonal class (4/mmm), directional Young's modulus E along the unit vector l_i may be expressed as (Eq 21) [33]

$$E = \left[\left(l_1^4 + l_2^4 \right) S_{11} + \left(1 - l_3^2 \right) l_3^2 \left(S_{44} + 2S_{13} \right) + l_1^2 l_2^2 \left(S_{66} + 2S_{12} \right) + l_3^4 S_{33} \right]^{-1} \quad (21)$$

Here, l_1, l_2 and l_3 represent direction cosines.
S_{ij} symbolises the elastic compliance constants.
For all tetragonal crystal systems, the directional linear compressibility β along the unit vector l_i may be expressed as (Eq 22) [33]

$$\beta = \left(S_{11} + S_{12} + S_{13} \right) - \left(S_{12} - S_{13} + S_{11} - S_{33} \right) l_3^2 \quad (22)$$

Using the data of Table 1, variation of Young's modulus (along [100] and [001] crystallographic directions) of α-ZnP_2 with pressure is shown in Figure 3(a). It is clear from Figure 3(a) that $E_{[100]}$ and $E_{[001]}$ increase and then decrease with pressure in the pressure range of 0 to 10 GPa. Young's modulus $E_{[001]}$ at pressure of 10 GPa is greater than $E_{[001]}$ at zero pressure, whereas $E_{[100]}$ at a pressure of 10 GPa is less than $E_{[100]}$ at zero pressure. As α-ZnP_2 crystal has tetragonal symmetry (a≠c), therefore, it is also expected that values of Young's modulus along [100] and [001] are not the same.

Using our computed elastic stiffness constants (Table 1 data) of α-ZnP_2 at different pressures, minimum and maximum of shear modulus G and Young's modulus E are estimated using ELATE software [34–35]. The variations of the maximum (G_{max} and E_{max}) and minimum (G_{min} and E_{min}) of G and E are shown in Figure 3(b) in the pressure range 0-10 GPa. As pressure increases, the differences E_{max}–E_{min} and G_{max}–G_{min} increase with pressure. It suggests the increase of elastic anisotropy with increasing pressure. The rate of change of E_{max} with pressure is greater than that of E_{min}, G_{max} and G_{min}.

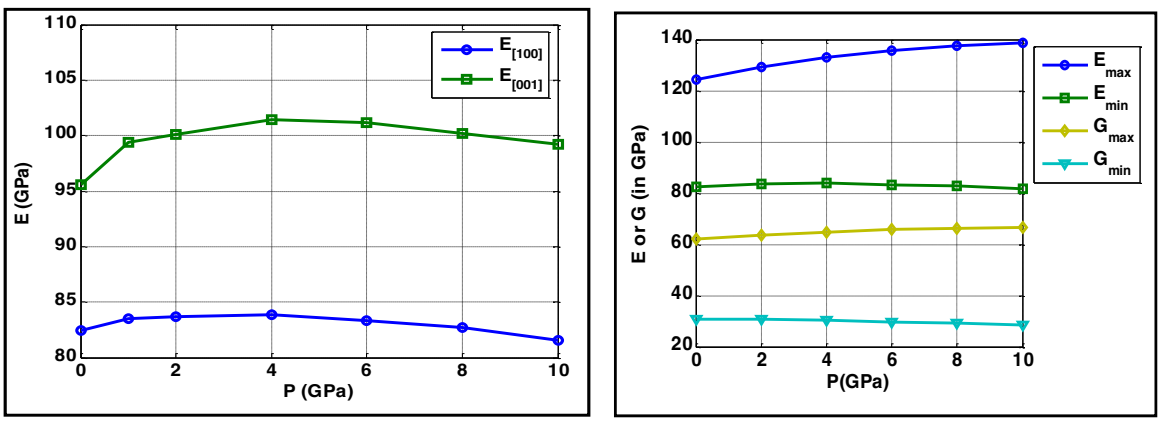

(a) (b)

Figure 3. Variation of: **(a)** Young's modulus E of α-ZnP_2 along different crystallographic directions with pressure; **(b)** minimum and maximum of Young's modulus E and shear modulus G of α-ZnP_2 with pressure

For representing the degree of elastic anisotropy, Ranganathan *et al.* [48] presented the universal elastic anisotropy index in the following approach shown in (Eq 23)

$$A^{U} = \frac{B_V}{B_R} + 5\frac{G_V}{G_R} - 6 \tag{23}$$

A log-Euclidean anisotropy scheme is a different strategy to get the measure of elastic anisotropy of crystals, in which elastic anisotropy index is represented as shown in (Eq 24) [49]

$$A^{L} = \sqrt{\left[\ln\left(\frac{B_V}{B_R}\right)\right]^2 + 5\left[\ln\left(\frac{G_V}{G_R}\right)\right]^2} \tag{24}$$

The calculated values of A^U and A^L for α-ZnP_2 crystals are represented in Figure 4. For the elastic-isotropic materials, values of A^U and A^L become zero [48–49]. It is evident from Figure 4 that increasing pressure results in increase in values of A^U and A^L. Figure 4 also explains the ratio of the maximum to minimum of elastic quantities.

At pressures P=0 and P=10 GPa, polar plots (2D) of Young's modulus and linear compressibility are depicted in Figure 5 and Figure 6, respectively, using data of Table 1. The angular variation of E is similar in the (010) plane and in the (100) plane. At zero pressure, in the $(1\bar{1}0)$ plane, Young's modulus E increases continuously from 95.57 GPa to 124.35 GPa as the angle (with [001] direction) increases from 0° to 90°. At zero pressure, for planes (001) and $(1\bar{1}0)$, the maximum percentage changes in Young's modulus E relative to their respective minimum values (in the corresponding planes) are 50.9% and 30.1%, respectively. In the (001) plane, at an angle of 45° to [100] direction, the maximum change in value of E takes place with a change in pressure.

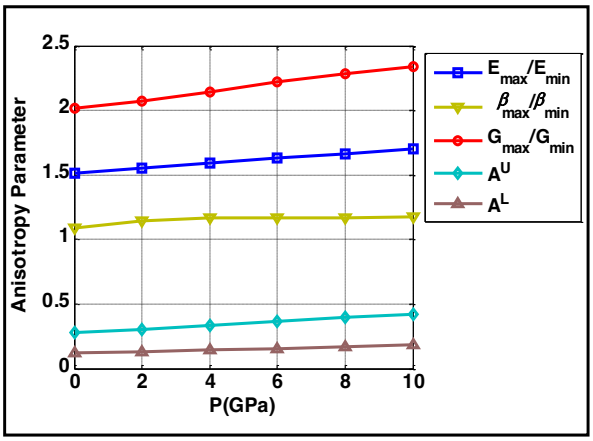

Figure 4. Elastic anisotropy parameters of α-ZnP_2 with pressure

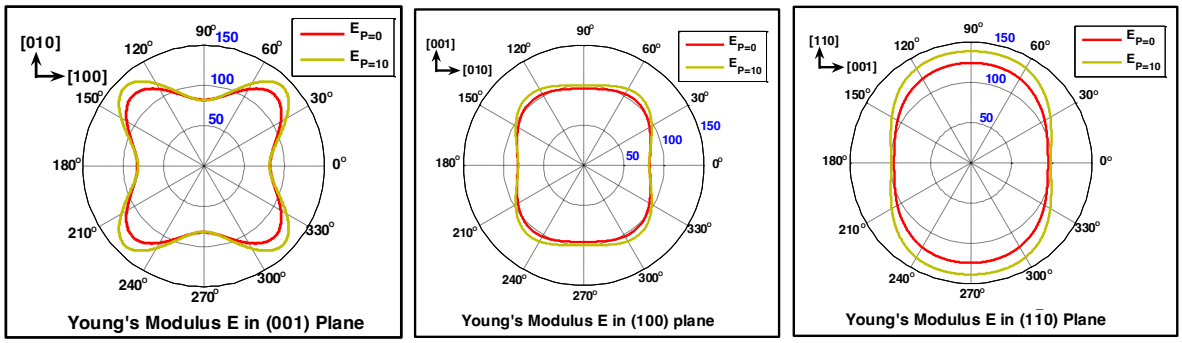

(a) **(b)** **(c)**

Figure 5. Representation (2D directional polar graphs) of Young's modulus E (in GPa units) of α-ZnP_2 at pressures P=0 and P=10 GPa. Projections of Young's modulus E on: **(a)** the (001) plane, **(b)** the (100) plane **(c)** the (1$\bar{1}$0) plane

The angular variation of linear compressibility β is similar in the (010) plane and in the (1$\bar{1}$0) plane. Thus, in the case of linear compressibility, the (010) and (1$\bar{1}$0) planes have higher anisotropy compared to the (001) plane. For the tetragonal crystal symmetry (a=b), linear compressibility is represented by a circular shape in xy-plane for the polar graphs.

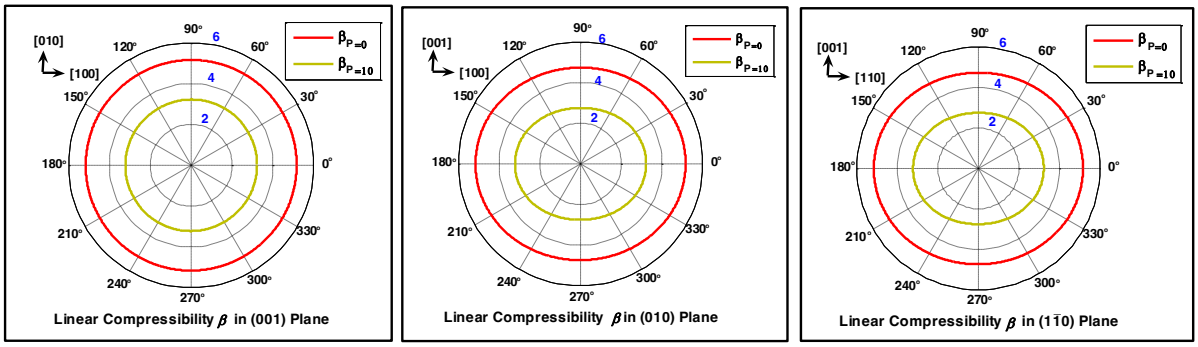

(a) **(b)** **(c)**

Figure 6. Representation (2D directional polar graphs) of linear compressibility β [in $(TPa)^{-1}$ units] of α-ZnP_2 at pressures P=0 and P=10 GPa. Projections of linear compressibility β on: **(a)** the (001) plane, **(b)** the (010) plane **(c)** the (1$\bar{1}$0) plane

3D directional polar graphs of α-ZnP_2 for linear compressibility and Young's modulus at pressure P=10 GPa are plotted in Figure 7.

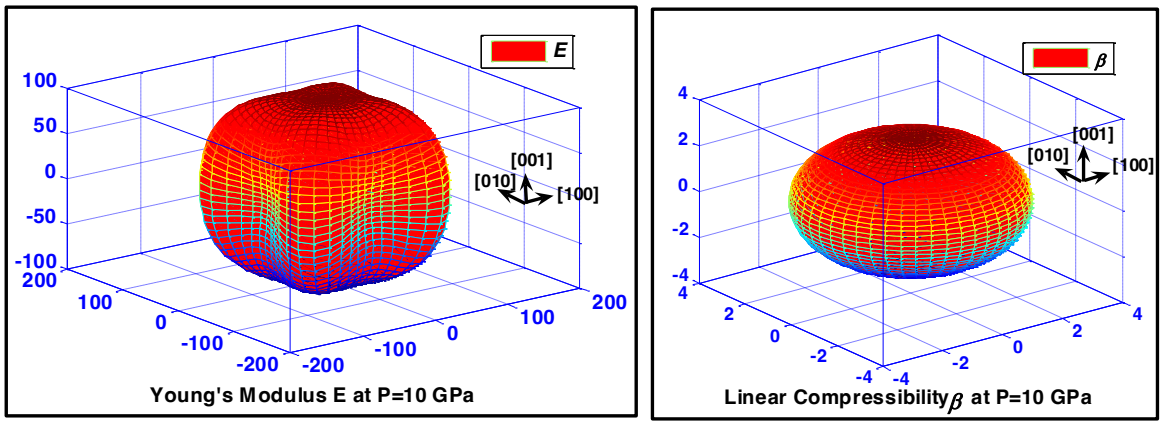

(a) **(b)**

Figure 7. For α-ZnP_2 at pressure P=10 GPa, representation (3D directional polar graphs) of: **(a)** Young's modulus E [in GPa units]; **(b)** linear compressibility β [in $(TPa)^{-1}$ units]

4. Conclusions

Our present study shows that bulk modulus is more responsive to applied pressure compared to shear modulus and Young's modulus. Our research reveals that values of B/G greater than 1.75 occur at pressures greater than around 2.3 GPa; therefore, the malleability of polycrystalline α-ZnP_2 increases with increasing pressure. The Poisson's ratio varies from 0.235 to 0.326 as pressure varies from 0 to 10 GPa.

The present findings reveal that α-ZnP_2 crystal system has specific elastic anisotropy. Planes (010) and $(1\bar{1}0)$ exhibit higher elastic anisotropy compared to the (001) plane for linear compressibility. In general, elastic anisotropy of the alpha phase of ZnP_2 increases as pressure increases. These results will be useful for experminentalists in understanding the variation of elastic anisotropy with pressure to achieve optimum performance and high durability of devices made from α-ZnP_2 crystals. As our present computational work is based on the DFT, and subsequent future experimental research is to be carried out to further validate the present findings.

Multidisciplinary Domains

This research covers the domains: (a) Physics, (b) Chemistry, (c) Materials Science.

Funding

This research received no external funding.

Acknowledgments

The authors acknowledge the University of Kota, Kota and Vardhman Mahaveer Open University, Kota for support. Authors are thankful to Department of Chemistry, University of Torino, Torino (Italy) for CRYSTAL Code.

Conflicts of Interest

The authors declare no conflict of interest.

Declaration on AI Usage

The authors declare that the article has been prepared without the use of AI tools.

References

[1] Oh, S.H.; Kim, Y.; Cubic ZnP_2 nanowire growth catalysed by bismuth. *Cryst. Eng. Comm.* **2021**, 23(11), 2297–2303, https://doi.org/10.1039/D1CE00029B

[2] Dutkiewicz, J.; The P-Zn (Phosphorus-Zinc) system. *J. Phase Equilib.* **1991**, 12(4), 435–438, https://doi.org/10.1007/BF02645963

[3] Ghasemi, M.; Stutz, E.; Steinvall, S.E.; Zamani, M.; Fontcuberta i Morral, A.; Thermodynamic re-assessment of the ZnP binary system. *Materialia* **2019**, 6, 100301, https://doi.org/10.1016/j.mtla.2019.100301

[4] Zdanowicz, W.; Zdanowicz, L.; Semiconducting Compounds of the A^{II} B^{V} Group. *Annu. Rev. Mater. Res.* **1975**, 5, 301–328, https://doi.org/10.1146/annurev.ms.05.080175.001505

[5] Hegyi, I.J.; Loebner, E.E; Poor Jr., E.W.; White, J.G.; Two crystal forms of ZnP_2, their preparation, structure, and optoelectronic properties. *J. Phys. Chem. Solids* **1963**, 24(2), 333–337, https://doi.org/10.1016/0022-3697(63)90140-9

[6] White, J.G.; The Crystal Structure of the Tetragonal Modification of ZnP_2. *Acta Crystallogr.* **1965**, 18(2), 217–220, https://doi.org/10.1107/S0365110X6500049X

[7] Stackelberg, M.V.; Paulus, R.; Untersuchungen an den Phosphiden und Arseniden des Zinks und Cadmiums. Das Zn_3P_2-Gitter. *Z. Phys. Chem.* **1935**, 28B(1), 427–460, https://doi.org/10.1515/zpch-1935-2841

[8] Zanin, I.E.; Aleinikova, K.B; Antipin, M.Y; Analysis of Chemical Bonding in the α and β Modifications of Zinc Diphosphide from X-ray Diffraction Data. *Crystallogr. Rep.* **2003**, 48(2), 199–204, https://doi.org/10.1134/1.1564195

[9] Rubenstein, M.; Dean, P.J.; Preparation of Zinc Diphosphides and the Low-Temperature Luminescence and Absorption of the Tetragonal Polymorph. *J. Appl. Phys.* **1970**, 41(4), 1777–1786, https://doi.org/10.1063/1.1659103

[10] Živković, A.; Farkaš, B.; Uahengo, V.; de Leeuw, N.H.; Dzade, N.Y.; First-principles DFT insights into the structural, elastic, and optoelectronic properties of α and β-ZnP_2: implications for photovoltaic applications. *J. Phys. Condens. Matter* **2019**, 31(26), 265501, https://doi.org/10.1088/1361-648X/ab111c

[11] Fan, C.L.; Cheng, X.L.; Zhang, H.; First-principles study of the structural and electronic properties of the α modification of zinc diphosphide. *Phys. Status Solidi B* **2009**, 246(1), 77–81, https://doi.org/10.1002/pssb.200844007

[12] Yang, Z.; Wang, X.; Liu, L.; Yang, S.; Su, X.; Density functional theory studies on elastic and electronic properties of tetragonal ZnP_2. *Solid State Sci.* **2011**, 13(8), 1604–1607, https://doi.org/10.1016/j.solidstatesciences.2011.06.008

[13] Huang, H.M.; Li, Y.L.; Zeng, Z.; Structural, elastic, and electronic properties of compressed ZnP_2. *Physica B Condens. Matter* **2013**, 419, 112–115, https://doi.org/10.1016/j.physb.2013.03.036

[14] Litvinchuk, A.P.; Valakh, M.Y.; Raman and infrared phonons in tetragonal ZnP_2 and CdP_2 crystals: a density functional study. *J. Phys. Condens. Matter* **2020**, 32(44), 445401, https://doi.org/10.1088/1361-648X/aba720

[15] Farkaš, B.; Živković, A.; Uahengo, V.; Dzade, N.Y.; De Leeuw, N.H.; Insights from density functional theory calculations into the effects of the adsorption and dissociation of water on the surface properties of zinc diphosphide (ZnP_2) nanocrystals. *Phys. Chem. Chem. Phys.* **2021**, 23(46), 26482–26493, https://doi.org/10.1039/D1CP02784K

[16] Nam, K.H.; Hwa, Y.; Park, C.M.; Zinc Phosphides as Outstanding Sodium-Ion Battery Anodes. *ACS Appl. Mater. Interfaces* **2020**, 12(13), 15053–15062, https://doi.org/10.1021/acsami.9b21803

[17] Ji, S.; Song, C.; Li, J.; Hui, K.S.; Deng, W.; Wang, S.; Li, H.; Dinh, D.A.; Fan, X.; Wu, S.; Zhang, J.; Chen, F.; Shao, Z.; Hui, K.N.; Metal phosphides embedded with in situ-formed metal phosphate impurities as buffer materials for high-performance potassium-ion batteries. *Adv. Energy Mater.* **2021**, 11(40), 2101413, https://doi.org/10.1002/aenm.202101413

[18] Patskun, I.I.; Pavlova, N.Y.; Band structure of α-ZnP_2 studied by laser modulation spectroscopy. *Opt. Spectrosc.* **2004**, 96(1), 66–69, https://doi.org/10.1134/1.1643987

[19] Dorogan, A.V.; Beril, S.I.; Stamov, I.G.; Syrbu, N.N.; Me-ZnP_2 Diodes Sensible to Optical Gyration. *4th ICNBME* **2019**, *Chisinau, Moldova, IFMBE Proceedings*, Springer Cham, 77, 167–171, https://doi.org/10.1007/978-3-030-31866-6_34

[20] Stamov, I.G.; Syrbu, N.N.; Dorogan, A.V.; Photodetectors and birefringence in ZnP_2– C_{2h}^5 crystals. *Physica B Condens. Matter* **2013**, 412, 130–137, https://doi.org/10.1016/j.physb.2012.11.033

[21] Dovesi, R.; Erba, A.; Orlando, R.; Zicovich-Wilson, C.M.; Civalleri, B.; Maschio, L.; Rérat, M.; Casassa, S.; Baima, J.; Salustro, S.; Kirtman, B.; Quantum-Mechanical Condensed Matter Simulations with CRYSTAL. *WIREs Comput. Mol. Sci.* **2018**, 8(4), e1360, https://doi.org/10.1002/wcms.1360

[22] Dovesi, R.; Saunders, V.R.; Roetti, C.; Orlando, R.; Zicovich-Wilson, C.M.; Pascale, F.; Civalleri, B.; Doll, K.; Harrison, N.M.; Bush, I.J.; D'Arco, P.; Llunell, M.; Causà, M.; Noël, Y.; Maschio, L.; Erba, A.; Rérat, M.; Casassa, S.; *CRYSTAL17 User's Manual*, University of Torino, Torino, **2017.**

[23] Erba, A.; Mahmoud, A.; Belmonte, D.; Dovesi, R.; High pressure elastic properties of minerals from *ab initio* simulations: The case of pyrope, grossular and andradite silicate garnets. *J. Chem. Phys.* **2014**, 140(12), 124703, https://doi.org/10.1063/1.4869144

[24] Perger, W.F.; Criswell, J.; Civalleri, B.; Dovesi, R.; Ab-initio calculation of elastic constants of crystalline systems with the CRYSTAL code. *Comput. Phys. Commun.* **2009**, 180(10), 1753–1759, https://doi.org/10.1016/j.cpc.2009.04.022

[25] Erba, A.; Mahmoud, A.; Orlando, R.; Dovesi, R.; Elastic properties of six silicate garnet end members from accurate ab initio simulations. *Phys. Chem. Miner.* **2014**, 41(2), 151–160, https://doi.org/10.1007/s00269-013-0630-4

[26] Perdew, J.P.; Burke, K.; Ernzerhof, M.; Generalized Gradient Approximation Made Simple. *Phys. Rev. Lett.* **1996**, 77(18), 3865–3868, https://doi.org/10.1103/PhysRevLett.77.3865

[27] Perdrew, J.P.; Burke, K.; Ernzerhof, M.; Erratum: Generalized Gradient Approximation Made Simple [*Phys. Rev. Lett.,* 77, 3865 (1996)]. *Phys. Rev. Lett.* **1997**, 78(7), 1396, https://doi.org/10.1103/PhysRevLett.78.1396

[28] Vilela Oliveira, D.; Laun, J.; Peintinger, M.F.; Bredow, T.; BSSE-Correction Scheme for Consistent Gaussian Basis Sets of Double-and Triple-Zeta Valence with Polarization Quality for Solid-State Calculations. *J. Comput. Chem.* **2019**, 40(27), 2364–2376, https://doi.org/10.1002/jcc.26013

[29] Zicovich-Wilson, C.M.; Bert, A.; Roetti, C.; Dovesi, R.; Saunders, V.R.; Characterization of the electronic structure of crystalline compounds through their localized Wannier functions. *J. Chem. Phys.* **2002**, 116(3), 1120–1127, https://doi.org/10.1063/1.1425406

[30] Broyden, C.G.; A Class of Methods for Solving Nonlinear Simultaneous Equations. *Math. Comput.* **1965**, 19(92), 577–593, https://doi.org/10.1090/S0025-5718-1965-0198670-6

[31] Johnson, D.D.; Modified Broyden's method for accelerating convergence in self-consistent calculations. *Phys. Rev. B* **1988**, 38(18), 12807–12813, https://doi.org/10.1103/PhysRevB.38.12807

[32] Monkhorst, H.J.; Pack, J.D.; Special points for Brillouin-zone integrations. *Phys. Rev. B* **1976**, 13(12), 5188–5192, https://doi.org/10.1103/PhysRevB.13.5188

[33] Nye, J.F.; Physical Properties of Crystals: Their Representation by Tensors and Matrices.**,** Oxford University Press Inc.: New York, **1985.**

[34] Gaillac, R.; Pullumbi, P.; Coudert, F.X.; ELATE: An open-source online application for analysis and visualization of elastic tensors. *J. Phys. Condens. Matter* **2016**, 28(27), 275201, https://doi.org/10.1088/0953-8984/28/27/275201

[35] http://progs.coudert.name/elate

[36] Rajpurohit, S.; Ab-Initio Investigation of Structural, Electronic and Elastic Properties of Some II-V_2 Semiconducting Compounds, Ph.D. Thesis, University of Kota, Kota, **April 2025**.

[37] https://crysplot.crystalsolutions.eu/

[38] Beata, G.; Perego, G.; Civalleri, B.; CRYSPLOT: A new tool to visualize physical and chemical properties of molecules, polymers, surfaces, and crystalline solids. *J. Comput. Chem.* **2019**, 40(26), 2329–2338, https://doi.org/10.1002/jcc.25858

[39] Soshnikov, L.E.; Trukhan, V.M.; Golyakevich, T.V.; Soshnikova, H.L.; Elastic and dielectric properties of $A^{II} B_2^{V}$ (A= Cd or Zn, B= P or As) single crystals. *Crystallogr. Rep.* **2005**, 50(1), S37–S45, https://doi.org/10.1134/1.2133970

[40] Mouhat, F.; Coudert, F.X.; Necessary and sufficient elastic stability conditions in various crystal systems. *Phys. Rev. B* **2014**, 90(22), 224104, https://doi.org/10.1103/PhysRevB.90.224104

[41] Voigt, W.; Lehrbuch der Kristallphysik. BG Teubner: Leipzig and Berlin, **1928**.

[42] Reuss, A.; Berechnung der Fliesgrenze von Mischkristallen auf Grund der Plastizatsberechnung fur Einkristalle. *J. Appl. Math. Mech.* **1929**, 9(1), 49–58, https://doi.org/10.1002/zamm.19290090104

[43] Hill, R.; The Elastic Behaviour of a Crystalline Aggregate. *Proc. Phys. Soc. A* **1952**, 65(5), 349–354, https://doi.org/10.1088/0370-1298/65/5/307

[44] Kikegawa, T.; Iwasaki, H.; An X-ray diffraction study of lattice compression and phase transition of crystalline phosphorus. *Acta Crystallogr. Sec. B* **1983**, 39(2), 158–164, https://doi.org/10.1107/S0108768183002220

[45] Warlimont, H.; Martienssen, W. (Eds.); Springer Handbook of Materials Data. 2nd ed. Springer Nature: Cham, Switzerland, **2018**, https://doi.org/10.1007/978-3-319-69743-7

[46] Pugh, S.F.; XCII. Relations between the Elastic Moduli and the Plastic Properties of Polycrystalline Pure Metals. *Lond. Edinb. Dubl. Phil. Mag. & J. Sci.* **1954**, 45(367), 823–843, https://doi.org/10.1080/14786440808520496

[47] Love, A.E.H.; A Treatise on the Mathematical Theory of Elasticity. Cambridge University Press: Cambridge, **1892.**

[48] Ranganathan, S.I.; Ostoja-Starzewski, M.; Universal Elastic Anisotropy Index. *Phys. Rev. Lett.* **2008**, 101(5), 055504, https://doi.org/10.1103/PhysRevLett.101.055504

[49] Kube, C.M.; Elastic anisotropy of crystals. *AIP Adv.* **2016**, 6(9), 095209, https://doi.org/10.1063/1.4962996